Patterns of convection in a mushy layer

S.R. Keating

March 15, 2007

Abstract

A solidification front advancing into a binary melt is often preceded by a mushy layer of fine dendritic crystals in thermodynamic equilibrium with solutal liquid in the interstices. One of the most striking features of such directional solidification — and most undesirable in industrial contexts — is the formation of vertical channels of zero solid fraction in the mushy layer. These "chimneys" are believed to form as a consequence of coupling between dissolution, solidification and compositional convection within the mush.

In this work, we extend the weakly nonlinear analysis of previous studies to the case of a continuous horizontal planform, in an effort to understand better the structure and spatial distribution of chimneys in a mushy layer. The relevent pattern equation is derived and has the form of a Swift-Hohenberg equation with an additional quadratic term. We show that this quadratic term is only present for the case of a hexagonal array of rolls and breaks the symmetry between up-flow and down-flow at the center of hexagons. Such symmetry-breaking is ultimately rooted in the non-Boussinesq solid-fraction dependence of the permeability within the mushy layer. Finally, we show that in a periodic domain the pattern equation exhibits localized structures which we interpret as nascent chimneys.

"Work is the curse of the drinking classes." -Oscar Wilde

"One of us has to go." -Oscar Wilde (last words, attrib.)

"Press On!" -EAS

1 Introduction

A mushy layer can be thought of as the means by which a solidification front adjusts to constitutional supercooling in a two-component melt. The mush itself is a forest of dendritic crystals – generated via morphalogical instability of the solid–liquid interface – in thermodynamic equilibrium with solutal liquid in the interstices. It can also be thought of as a reactive porous medium in which the solid fraction, and hence the permeability, is dynamically coupled to the flow. Mushy layers are found in a wide variety of situations in nature and industry: large alloy castings, sea ice, lava lakes and Earth's inner-core boundary are a few examples. For an overview of mushy layers and other issues in solidification theory, see Davis [1].

One of the most compelling features of mushy layers, and most undesirable in the context of industrial applications, is the formation of "chimneys" — quasi-vertical channels of zero solid fraction from which solute-poor residual liquid is expelled from the mush into the adjacent liquid region [2]. Such chimneys manifest themselves as "brine channels" in sea ice and are believed to give rise to "freckles" in alloy casting and geological formations.

Weakly nonlinear analysis of a simplified model of convection in a mushy layer was first carried out by Amberg & Homsy ([3]; hereafter AH93) and Anderson & Worster ([4]; hereafter AW95). In both of these treatments a discrete planform was assumed — three rolls of different amplitude were superimposed at 120 degrees to one another. In AW95 the relative stability of rolls (one non-zero amplitude), hexagons (three equal amplitudes) and mixed modes (three finite amplitudes, two equal) was calculated and it was concluded that there exists a transcritical bifurcation to hexagons.

AW95 also indicated the presence of a Hopf bifurcation, giving rise to an oscillatory instability examined in more detail in a later paper [5]. In constrast to an oscillatory instability detected earlier by Chen, Lu and Yang [6], and which owed its origin to double-diffusive convection in the liquid above, the instability of Anderson & Worster [5] is due to physical interactions internal to the mush itself. A number of authors have developed the theory of these oscillatory modes [7, 8, 9]. In this work, we shall focus attention on the direct mode, leaving its extension to the oscillatory case a subject for future research.

In this work we ask the following question: what determines the structure and spatial distribution of the chimneys? This article proceeds as follows: we briefly review the formulation of AH93 and AW95 in section 2 and the linear theory of Anderson & Worster [5] in section 3. In section 4 we extend the weakly nonlinear analysis of AW95 to the case of a continuous horizontal planform and derive the relevant pattern equation. In section 5, we calculate explicit expressions for the coefficients appearing in the pattern equation in terms of the physical parameters of the sytem for the near-marginal case of an infinitesimally thin band of wavenumbers centred on the critical value. We show in section 6 that the general, stationary pattern equation possesses solutions with localized structure and interpret these as nascent chimneys. Finally, in section 7 we discuss our results.

2 Formulation

We outline here the formulation of AH93 and subsequent studies [4, 5, 7, 8, 9, 10, 11], as depicted in fig.(1). The mush is modelled as a single porous layer sandwiched between liquid above and solid below. For mathematical expedience we prescribe a constant solidification speed V and assume that the mush is dynamically decoupled from both the liquid and the solid. These and subsequent assumptions are considered in detail in the references cited above and will not be discussed further here. It is sufficient to note that, while the assumptions simplify the analysis considerably, they preserve the essential physical interactions of interest.

It is assumed that, within the mushy layer, interstitial liquid is in thermodynamic equilibrium with fine-grained dendritic crystals, so that the temperature and solute fields are coupled via a liquidus relation

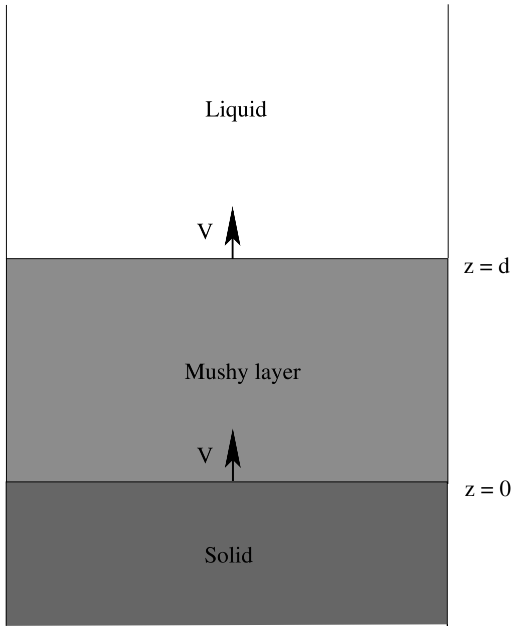

Figure 1: The model system. A solidification front advances into a binary alloy at a rate V. A mushy layer of thickness d is sandwiched between the two regions and advances with the front. The solid is at the eutectic temperature T_E and solid composition C_S; the liquid region is at the far-field composition C_0 and associated liquidus temperature $T_L(C_0)$. See text and references for further discussion.

$$T = T_L(C). \tag{1}$$

The far-field composition C_0 and temperature T_∞ are taken to be above the eutectic composition ($C_0 > C_E$), and above the far-field liquidus temperature ($T_\infty > T_L(C_0)$), respectively. The temperature field T, solid fraction ϕ, fluid velocity $\mathbf{u}$ and pressure p within the mushy layer are then governed by equations describing heat balance, solute balance, Darcy's law for flow in a porous medium, and mass continuity; the non-dimensional ideal mushy layer equations in a reference frame moving with the solidification front are given by Worster [12] as

$$\begin{aligned}
(\partial_t - \partial_z)(\theta - \mathcal{S}\phi) + \mathbf{u}\cdot\nabla\theta &= \nabla^2\theta, && (2)\\
(\partial_t - \partial_z)((1-\phi)\theta + \mathcal{C}\phi) + \mathbf{u}\cdot\nabla\theta &= 0, && (3)\\
\mathcal{K}(\phi)\mathbf{u} &= -\nabla p - Ra\theta\hat{\mathbf{z}}, && (4)\\
\nabla\cdot\mathbf{u} &= 0. && (5)
\end{aligned}$$

The non-dimensional temperature field (or, via the liquidus relation (1), the compositional field) is

$$\theta = \frac{T - T_L(C_0)}{T_L(C_0) - T_E} = \frac{C - C_0}{C_0 - C_E}, \tag{6}$$

Symbol	Physical Quantity	Symbol	Physical Quantity
L	Latent heat	β	Expansion coefficient
c_l	Specific heat	g	Gravitational acceleration
T_E	Eutectic temperature	$\Pi(0)$	Permeability at zero solid-fraction
T_∞	Far-field temperature	κ	Thermal diffusivity
C_E	Eutectic composition	ν	Kinematic viscosity
C_0	Far-field composition	d	Mushy layer thickness
C_S	Solid composition	V	Speed of solidification front

Table 1: Physical quantities appearing in the dimensionless parameters $\mathcal{S}$, $\mathcal{C}$ and Ra, and the mushy layer equations (2-5). For further details see cited references.

while lengths, times and velocities in (2-5) have been scaled with κ/V, κ/V^2 and V respectively, with κ as the thermal diffusivity. The function $\mathcal{K}(\phi)$ appearing in equation (4) measures the variation of permeability $\Pi(\phi)$ with solid fraction, with respect to some zero-solid-fraction permeability $\Pi(0)$, assumed finite:

$$\mathcal{K}(\phi) = \frac{\Pi(0)}{\Pi(\phi)}. \tag{7}$$

The dimensionless parameters appearing in (2-5) are the Stefan number

$$\mathcal{S} = \frac{L}{c_l\left(T_L(C_0) - T_E\right)}, \tag{8}$$

the concentration ratio

$$\mathcal{C} = \frac{C_S - C_0}{C_0 - C_E}, \tag{9}$$

and the Rayleigh number

$$Ra = \frac{\beta\left(C_0 - C_E\right) g \Pi(0)\, \kappa/V}{\nu\kappa}. \tag{10}$$

The various physical quantities appearing in (8–10) are listed in table (1). Futher discussion of these parameters and their physical significance can be found in the references cited above.

A fourth dimensionless parameter, the dimensionless mush thickness $\delta = d/(\kappa/V)$, appears in the boundary conditions:

$$\theta = -1, w = 0 \quad \text{on } z = 0, \tag{11}$$

$$\theta = 0, w = 0, \phi = 0 \quad \text{on } z = \delta. \tag{12}$$

Boundary conditions (11) and (12) correspond to impermeable rigid plates co-moving with the upper and lower boundary of the mushy layer. The lower plate, between the solid and the mush, is maintained at the eutectic temperature T_E, while the upper boundary between the liquid and the mush (that is, at zero solid fraction ϕ), is maintained at the far-field liquidus temperature $T_L(C_0)$.

A more physically plausible kinematic upper boundary condition might be one of constant pressure p. Chung and Chen [10] considered a stress-free upper boundary condition and, while their analysis was much more involved than that of AH93 and AW95, no qualitatively new results were uncovered. We therefore proceed with confidence that the boundary conditions (11) and (12) preserve the interactions of interest without undue complication.

To isolate a parameter regime for which there is a physically interesting interplay between dissolution, solidification and convection we adopt the following additional scalings: we consider a thin mushy layer ($\delta \ll 1$) [3]; we assume a near-eutectic approximation ($\mathcal{C} = \bar{C}/\delta = O\left(\delta^{-1}\right)$) [13]; and we assume a large Stefan number ($\mathcal{S} = \bar{S}/\delta = O\left(\delta^{-1}\right)$) [4]. The reader may consult the cited references for further details on these scalings. We note in passing, however, that a key implication of the near-eutectic approximation ($\mathcal{C} = O\left(\delta^{-1}\right)$) is that the solid fraction is small, and hence the permeability is uniform to lowest order. As a consequence, we follow AH93 and expand the permeability in the small solid fraction:

$$\mathcal{K}\left(\phi\right) = 1 + \mathcal{K}_1\phi + \mathcal{K}_2\phi^2 + \cdots \tag{13}$$

where, on physical grounds, we demand that $\mathcal{K}_1$, $\mathcal{K}_2$, etc. are non-negative.

3 Linear theory

We continue to follow AH93 and AW95 and rescale space and time as

$$\mathbf{x} \rightarrow \delta\mathbf{x}, \tag{14}$$
$$t \rightarrow \delta^2 t, \tag{15}$$

and introduce the effective Rayleigh number

$$R^2 = \delta Ra. \tag{16}$$

Note that, following the notation of AH93 and AW95, R is the *square root* of the effective Rayleigh number.

The dynamical fields θ, ϕ, $\mathbf{u}$ and p are separated into a stationary basic state and a perturbation:

$$\begin{aligned}
\theta &\rightarrow \theta_B\left(z\right) + \epsilon\theta\left(\mathbf{x}, t\right), \\
\phi &\rightarrow \phi_B\left(z\right) + \epsilon\phi\left(\mathbf{x}, t\right), \\
\mathbf{u} &\rightarrow \mathbf{0} + \epsilon\mathbf{u}\left(\mathbf{x}, t\right), \\
p &\rightarrow p_B\left(z\right) + \epsilon p\left(\mathbf{x}, t\right),
\end{aligned} \tag{17}$$

where the subscript 'B' denotes the basic state and ϵ is the amplitude of the perturbations. Subtracting the basic states from the equations of motion and eliminating the pressure p via the incompressibility condition, we obtain the equations for the perturbations θ, ϕ and $\mathbf{u}$:

$$
\begin{aligned}
\left(\delta\partial_z - \epsilon^2\partial_T\right)\left(\theta - \frac{\bar{S}}{\delta}\phi\right) - R'\theta_B'(z)\,w + \nabla^2\theta &= \epsilon R\mathbf{u}\cdot\nabla\theta,\\
\left(\delta\partial_z - \epsilon^2\partial_T\right)\left(\left(1 - \delta\bar{\phi_B}(z) - \epsilon\phi\right)\theta - \left(\theta_B - \frac{\bar{C}}{\delta}\right)\phi\right) - R\theta_B'(z)\,w &= \epsilon R\mathbf{u}\cdot\nabla\theta,\\
\nabla^2(\mathcal{K}u) - \partial_x(\mathbf{u}\cdot\nabla\mathcal{K}) - R\partial_x\partial_z\theta &= 0,\\
\nabla^2(\mathcal{K}v) - \partial_y(\mathbf{u}\cdot\nabla\mathcal{K}) - R\partial_y\partial_z\theta &= 0,\\
\nabla^2(\mathcal{K}w) - \partial_z(\mathbf{u}\cdot\nabla\mathcal{K}) + R\nabla_2^2\theta &= 0,\\
\nabla\cdot\mathbf{u} &= 0.
\end{aligned} \tag{18}
$$

The equations of motion (18) can be written as

$$
(\mathcal{L} - \mathcal{T}\partial_t)\,\mathbf{v} = \epsilon\mathbf{N}, \tag{19}
$$

where $\mathbf{v} = \{\theta,\, \phi,\, \mathbf{u}\}$ is the vector of perturbed fields, $\mathcal{L} - \mathcal{T}\partial_t$ is the linear operator. We discard the nonlinearity $\mathbf{N}$ by setting ϵ to zero, and look for solutions of the form $\mathbf{v}_{0k\sigma}(z)\exp(i\mathbf{k}\cdot\mathbf{x} + \sigma t)$ satisfying

$$
(\mathcal{L}_{0k} - \sigma\mathcal{T}_{0k})\,\mathbf{v}_{0k\sigma} = 0. \tag{20}
$$

Here, $\mathbf{k} = (k_x,\, k_y)$ and $\mathbf{x} = (x,\, y)$. Note that, as a consequence of the assumption that $\mathcal{K}_1 = O(\epsilon)$, variations in the permeability appear only at higher order.

The matrix operators $\mathcal{L}_{0k}$ and $\mathcal{T}_{0k}$, the linear fields $\mathbf{v}_{0k\sigma}$, the growth rate σ and the basic states $\theta_B(z)$ and $\phi_B(z)$ can be expanded in powers of δ and the linear equation (20) solved perturbatively. Thus, we have

$$
\mathcal{L}_{0k}(z) = \mathcal{L}_{00} + \delta\mathcal{L}_{01} + \cdots \tag{21}
$$

$$
\mathbf{v}_{0k\sigma}(z) = \mathbf{v}_{00} + \delta\mathbf{v}_{01} + \cdots \tag{22}
$$

$$
\sigma = \sigma_0 + \delta\sigma_1 + \cdots \tag{23}
$$

$$
\phi_B(z) = -\delta\frac{z-1}{\bar{C}} - \delta^2\left(\frac{(z-1)^2}{\bar{C}^2} - \frac{z^2 - z}{2\bar{C}}\right) + \cdots \tag{24}
$$

$$
\theta_B(z) = (z-1) - \delta\frac{z^2 - z}{2} + \cdots \tag{25}
$$

We now substitute the expansions (21–25) into the linear equation (20) and at each order in δ obtain a linear ordinary differential equation for the linear fields $\mathbf{v}_{00}(z),\, \mathbf{v}_{01}(z)\cdots$. At $O\left(\delta^{-1}\right)$ we find

$$
\sigma_0\phi_{00} = 0, \tag{26}
$$

implying that $\sigma\phi_0 = O(\delta)$.

At $O\left(\delta^0\right)$, we find solutions

$$\theta_{00_k} = -f_k \sin\pi z, \qquad w_{00_k} = f_k \frac{|\mathbf{k}|}{\sqrt{\Omega}} \sqrt{1 + \frac{\Omega\sigma_0}{\pi^2 + k^2}} \sin\pi z, \tag{27}$$

$$u_{00_k} = \frac{ik_x}{k^2} w'_{00_k}, \quad v_{00_k} = \frac{ik_y}{k^2} w'_{00_k}, \tag{28}$$

where, as a consequence of incompressibility, the planform f_k satisfies

$$\nabla_H^2 f_k = -k^2 f_k, \tag{29}$$

and we have introduced $\Omega = 1 + \bar{S}/\bar{C}$. The zeroth-order growth rate is given by

$$\sigma_0 = \frac{\pi^2 + k^2}{\Omega} \left(\frac{R^2}{R_{00}^2(k)} - 1 \right), \tag{30}$$

where $R_{00}^2(k)$ describes the neutral curve

$$R_{00}^2(k) = \frac{\left(\pi^2 + k^2\right)^2}{\Omega k^2}. \tag{31}$$

The neutral curve (31) has a minimum of $4\pi^2/\Omega$ at $k_c = \pi$.

In addition to the solutions (27) and (28), we require the linear perturbation to the solid fraction ϕ_0. However, the condition (26) requires that we consider terms of higher order in δ. To lowest order,

$$\phi_{0k}(z) = -\frac{\pi^2 + k^2}{\Omega\bar{C}} \frac{\pi}{\pi^2 + (\sigma/\delta)^2} \left(\cos\pi z + \frac{\sigma}{\pi\delta} \sin\pi z + \mathrm{e}^{-\sigma(1-z)/\delta} \right) f_k. \tag{32}$$

Notice that this expression is valid for the case of both $\sigma = O(1)$ and $\sigma = O(\delta)$. In the former, condition (26) demands that $\phi_0 = O(\delta)$, while the latter implies that $\phi_0 = O(1)$. Anderson & Worster [5] showed that, for the case of $\sigma = O(\delta)$, the dispersion relation admits complex solutions, indicating the presence of an oscillatory instability. As we will be performing weakly nonlinear analysis near the marginal stability curve ($R = R_{00}(k) + O(\epsilon)$) in the asymptotic limit $\epsilon \ll \delta \ll 1$, we will be considering only the case of $\sigma = O(\delta)$, in which case (32) reduces to

$$\phi_{00k}(z) = -\frac{\pi^2 + k^2}{\Omega\bar{C}} \frac{\pi}{\pi^2 + \sigma_1^2} \left(\cos\pi z + \frac{\sigma_1}{\pi} \sin\pi z + \mathrm{e}^{-\sigma_1(1-z)} \right) f_k. \tag{33}$$

This is precisely the result of Anderson & Worster [5]. We shall employ this result for $\phi_{00k}(z)$ throughout our analysis.

4 Weakly nonlinear analysis

In this section, we perform a finite-amplitude perturbation expansion of the equations of motion in the spirit of AH93 and AW95. In contrast to these studies, and those of subsequent authors, we retain horizontal spatial information by considering a continuous horizontal planform rather than prescribing a discrete superposition of rolls. Again, unlike previous authors, we shall not *a priori* assume that the critical wavenumber k_c is the only mode excited. Rather, we consider a continuous band of wavenumbers, centred on k_c. In section 5, we restrict our attention to an infinitesimally thin band of wavenumbers, thus reproducing the results of previous studies. What is different about this approach is that we retain information about horizontal gradients in the amplitude equation thus obtained, and hence need make no *a priori* assumptions about the pattern. Note that in this calculation we do not rely upon a separation of scales to retain some slow spatial dependence of the amplitudes, as in standard derivations of the Ginzburg-Landau equation for example. Rather, spatial dependence is preserved in the wavenumber k, which is allowed to vary.

We follow AW95 and perform an asymptotic expansion in the ordered limit $\epsilon \ll \delta \ll 1$. That is, we first expand $\mathbf{v} = \{\theta, \phi, \mathbf{u}\}$ and R in ϵ; then, at each order, we expand in δ:

$$
\begin{aligned}
\mathbf{v} &= (\mathbf{v}_{00} + \delta\mathbf{v}_{01} + \cdots) + \epsilon\,(\mathbf{v}_{10} + \delta\mathbf{v}_{11} + \cdots) \\
&\qquad + \epsilon^2\left(\delta^{-1}\mathbf{v}_{2,-1} + \mathbf{v}_{20} + \delta\mathbf{v}_{21} + \cdots\right) + \cdots \qquad (34)\\
R &= (R_{00} + \delta R_{01} + \cdots) + \epsilon\,(R_{10} + \delta R_{11} + \cdots) \\
&\qquad + \epsilon^2\,(R_{20} + \delta R_{21} + \cdots) + \cdots \qquad (35)
\end{aligned}
$$

Notice that, as a consequence of $\mathcal{S}$, $\mathcal{C} = O\left(\delta^{-1}\right)$, we must include in the expansion the field $\mathbf{v}_{2,-1} = \{0, \phi_{2,-1}, \mathbf{0}\}$. It is also worthwhile noting that, because of the presence of a term of order $\epsilon^2\delta^{-1}$, the expansion (34) is singular in the limit $\delta \ll \epsilon \ll 1$, when the order is reversed.

We now substitute expansions (34) and (35) into the equations of motion (19) and look for slow time dependence $\partial_t = \epsilon^2\partial_T$. The perturbation expansion then proceeds as follows:

$$
\begin{aligned}
O\left(\epsilon^0\delta^0\right):&\quad \mathcal{L}_{00}\cdot\mathbf{v}_{00} &&= \mathbf{0},\\
O\left(\epsilon^0\delta^1\right):&\quad \mathcal{L}_{00}\cdot\mathbf{v}_{01} &&= -\mathcal{L}_{01}\cdot\mathbf{v}_{00},\\
\vdots\quad&\qquad\quad \vdots &&\ \ \vdots\\
O\left(\epsilon^1\delta^0\right):&\quad \mathcal{L}_{00}\cdot\mathbf{v}_{10} &&= -\mathcal{L}_{10}\cdot\mathbf{v}_{00} + \mathbf{N}_{10},\\
O\left(\epsilon^1\delta^1\right):&\quad \mathcal{L}_{00}\cdot\mathbf{v}_{11} &&= -\mathcal{L}_{11}\cdot\mathbf{v}_{00} - \mathcal{L}_{10}\cdot\mathbf{v}_{01} + \mathbf{N}_{11},\\
\vdots\quad&\qquad\quad \vdots &&\ \ \vdots\\
O\left(\epsilon^2\delta^{-1}\right):&\quad \mathcal{L}_{00}\cdot\mathbf{v}_{2,-1} &&= \mathcal{T}_{2,-1}\cdot\partial_T\mathbf{v}_{00},\\
O\left(\epsilon^2\delta^0\right):&\quad \mathcal{L}_{00}\cdot\mathbf{v}_{20} &&= \mathcal{T}_{2,-1}\cdot\partial_T\mathbf{v}_{01} + \mathcal{T}_{20}\cdot\partial_T\mathbf{v}_{00} - \mathcal{L}_{20}\cdot\mathbf{v}_{00}\\
& && \qquad -\mathcal{L}_{10}\cdot\mathbf{v}_{10} - \mathcal{L}_{01}\cdot\mathbf{v}_{2,-1} + \mathbf{N}_{20},\\
\vdots\quad&\qquad\quad \vdots &&\ \ \vdots
\end{aligned}
$$

At each step in the perturbation expansion, we obtain a system of linear, inhomogeneous ordinary differential equations of the form

$$\mathcal{L}_{00}\cdot\mathbf{v}_{mn} = \mathcal{I}_{mn}. \qquad (36)$$

As is well-known (see, for instance, [14, 15, 16]) a solution to (36) exists if and only if the inhomogeneities $\mathcal{I}_{mn}$ are orthogonal to the solutions $\tilde{\mathbf{v}}$ of the adjoint problem. That is,

$$\int_0^1 \mathrm{d}z \tilde{\mathbf{v}} \cdot \mathcal{I}_{mn} = 0. \tag{37}$$

In the present problem, neither the differential operator nor the boundary conditions is self-adjoint.

The solvability condition at $O\left(\epsilon^1 \delta^0\right)$ gives:

$$R_{10} \equiv 0. \tag{38}$$

This is a direct consequence of the assumption that $\mathcal{K}_1 = O\left(\epsilon\right)$.

The solvability condition at $O\left(\epsilon^2 \delta^0\right)$ gives the pattern equation for the planform f_k :

$$\lambda_k \partial_T f_k = \frac{2}{\sqrt{\Omega}} R_{20} \left|\mathbf{k}\right| f_k + \mathcal{M}\left\{f^2\right\} + \mathcal{N}\left\{f^3\right\}, \tag{39}$$

where

$$\mathcal{M}\left\{f^2\right\} \equiv \int \mathrm{d}\mathbf{p}\mathrm{d}\mathbf{q}\delta^2\left(\mathbf{k}-\mathbf{p}-\mathbf{q}\right)\mathcal{M}_{kpq} f_p f_q, \tag{40}$$

$$\mathcal{N}\left\{f^3\right\} \equiv \int \mathrm{d}\mathbf{l}\mathrm{d}\mathbf{m}\mathrm{d}\mathbf{n}\delta^2\left(\mathbf{k}-\mathbf{l}-\mathbf{m}-\mathbf{n}\right)\mathcal{N}_{klmn} f_l f_m f_n. \tag{41}$$

Here $\mathcal{M}_{kpq}$ and $\mathcal{N}_{klmn}$, the kernals of the integrals (40) and (41) are complicated functions of the horizontal wavevectors $\mathbf{k}$, $\mathbf{p}$, $\mathbf{q}$, $\mathbf{l}$, $\mathbf{m}$, and $\mathbf{n}$.

Close to marginality, the coefficient of the linear term on the right-hand side of (39) can be expressed as

$$\frac{2}{\sqrt{\Omega}} R_{20} \left|\mathbf{k}\right| \approx \frac{\pi^2 + k^2}{\Omega \epsilon^2}\left(\frac{R^2}{R_{00}^2\left(k\right)} - 1\right). \tag{42}$$

This is exactly the linear growth rate σ_0. Expanding about the critical wavenumber $k_c = \pi$ we find

$$\sigma_0 \approx \frac{2\pi^2}{\Omega\epsilon^2}\left(\frac{R^2 - R_c^2}{R_c^2} - \frac{1}{4}\left(\frac{k^2}{\pi^2} - 1\right)^2\right), \tag{43}$$

so that in real space the pattern equation for the planform $f = f\left(x, y\right)$ becomes

$$\lambda \partial_T f = \rho f - \left(\nabla_H^2 + 1\right)^2 f + \mu f^2 - \nu f^3. \tag{44}$$

This has of the form of a Swift-Hohenberg equation [17] with an addtional quadratic term. In (44), we have replaced the integrals $\mathcal{M}\left\{f^2\right\}$ and $\mathcal{N}\left\{f^3\right\}$ with numbers μf^2 and νf^3; we shall calculate explicit expressions for μ and ν in the following section.

5 Evaluation of the integrals

As discussed in section 4, the primary motivation for deriving a general pattern equation for a continuous planform f_k (or, in real space, $f(x, y)$) was to avoid making any *a priori* assumptions about the pattern. Rather, one can proscribe some arbitrary initial pattern (for instance, a random one) and, with the aid of a small computer, investigate its evolution. For Swift-Hohenberg-like pattern equations, one typically sees a number of patterns competing with one another until the planform settles into a fixed pattern and evolves no further. The final pattern generally falls into one of three categories: discrete rolls, hexagons (up or down), or labyrinths - which can be thought of as a planform frustrated between rolls and hexagons.

It is interesting to calculate explicit expressions for the coefficients μ and ν for discrete planforms. This is aided by the observation that, close to criticality the planforms f_p, f_q etc. are confined to a narrow band of wavenumbers centred on $k_c = \pi$, as depicted in fig. (2). Under these conditions it is possible to evaluate the integrals $\mathcal{M}\left\{f^2\right\}$ and $\mathcal{N}\left\{f^3\right\}$. That is, we assume that $f_p = f(\alpha)\,\delta(|\mathbf{p}| - \pi)$ where α is the angle $\mathbf{p}$ makes with $\mathbf{k} = k\hat{\mathbf{x}}$, without loss of generality. Under this assumption, all wavevectors must be of the same length and so only certain tessellations will satisfy the delta functions present in the integrands.

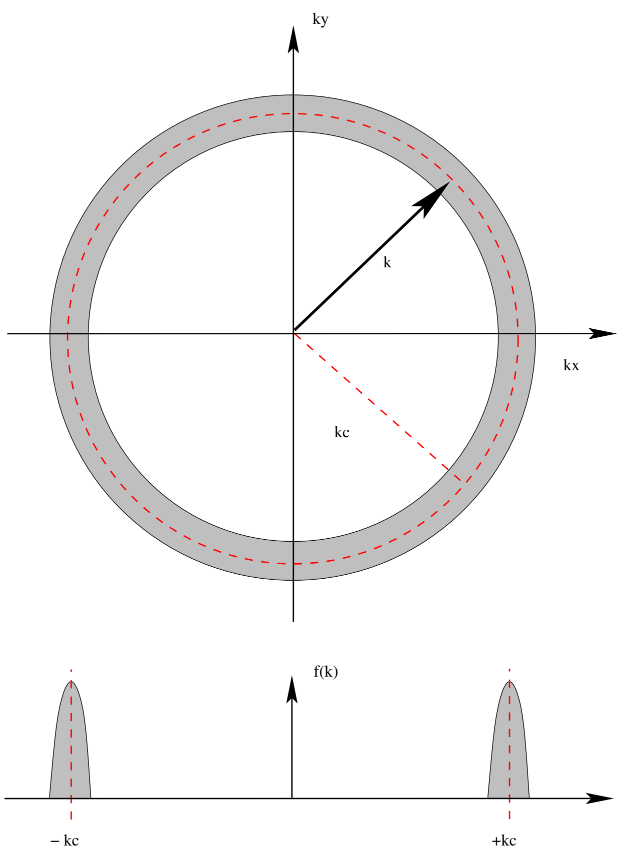

Figure 2: Support for f_k. We assume that f_k is confined to a narrow band of wavenumbers centred on $k_c = \pi$.

Concretely, the quadratic term $\mathcal{M}\left\{f^2\right\}$ in the pattern equation (44) is integrated over wavevector triads $\{\mathbf{k},\ \mathbf{p},\ \mathbf{q}\}$ satisfying the condition

$$\mathbf{k} = \mathbf{p} + \mathbf{q} \tag{45}$$

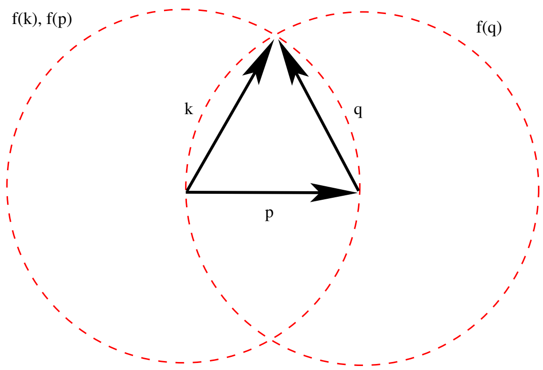

Figure 3: Allowed tesselations satisfying the condition $\mathbf{k} = \mathbf{p} + \mathbf{q}$. As $\mathbf{k}$, $\mathbf{p}$ and $\mathbf{q}$ are all of the same length ($k_c = \pi$), the triplet must form an equilateral triangle. Thus, the only planform possessing a quadratic term in its pattern equation is an "hexagonal array".

As all wavevectors are of the same length, the triad $\{\mathbf{k},\ \mathbf{p},\ \mathbf{q}\}$ must form an equilateral triangle. Consequently, the only planform possessing a quadratic term in its pattern equation is one with an equiangular array ("hexagonal array") of three superposed rolls, as depicted in fig. (3). This is the discrete case considered by AH93 and AW95. It is interesting to note that the appearance of a quadratic term is a special case of the more general pattern equation for a continuous planform.

We summarize this result as follows:

$$\begin{aligned} \mu f^2 \quad &= \pi^3 \left(\bar{\mathcal{K}}_1/\Omega\bar{C}\right) f\left(\tfrac{\pi}{3}\right) f^*\left(\tfrac{2\pi}{3}\right) && \text{for a hexagonal array,} \\ &= 0 && \text{otherwise,} \end{aligned} \tag{46}$$

where $f^*(\alpha) = f(\alpha + \pi)$.

In the case of the cubic term, the 4-tuple $\{\mathbf{k},\ \mathbf{l},\ \mathbf{m}\ \mathbf{n}\}$ must satisfy

$$\mathbf{k} = \mathbf{l} + \mathbf{m} + \mathbf{n}, \tag{47}$$

so that $\{\mathbf{k},\ \mathbf{l},\ \mathbf{m},\ \mathbf{n}\}$ form an equilateral parallelogram (fig. (4)). For general angle α between $\mathbf{k}$ and $\mathbf{l}$ (say), we find that

$$\begin{aligned} \nu f^3 \quad = \quad & \frac{8\pi^5}{9}\int_0^{2\pi} \mathrm{d}\alpha \left\{\frac{8}{5} + \frac{3-\cos\alpha}{9-4\cos\alpha}\left(1+\cos\alpha\right)^2 + \frac{3+\cos\alpha}{9+4\cos\alpha}\left(1-\cos\alpha\right)^2\right\} f(0)\left|f(\alpha)\right|^2 \\ & + \frac{22\pi^5}{3}\frac{\mathcal{K}_2}{\Omega^2\bar{C}^2}\int_0^{2\pi} \mathrm{d}\alpha f(0)\left|f(\alpha)\right|^2. \end{aligned} \tag{48}$$

As both rolls ($\alpha \equiv 0$) and hexagons ($\alpha \in \{0,\ \pi/3,\ 2\pi/3\}$) are special cases of (47), we expect the cubic term to appear in pattern equations for both planforms, with the coefficients

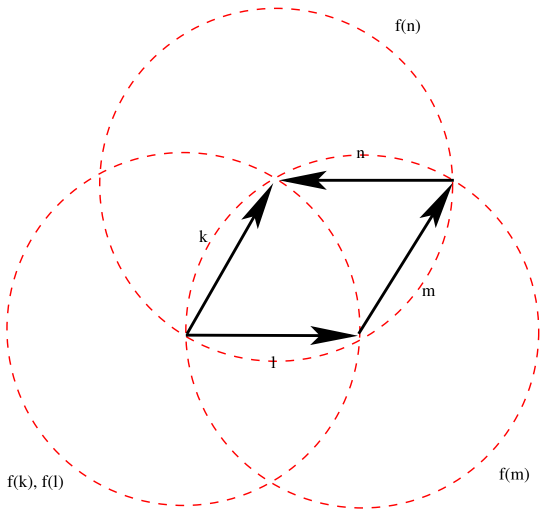

Figure 4: Allowed tesselations satisfying the condition $\mathbf{k} = \mathbf{l} + \mathbf{m} + \mathbf{n}$. The 4-tuple $\{\mathbf{k},\ \mathbf{l},\ \mathbf{m},\ \mathbf{n}\}$ forms an equilateral parallelogram. If all four wavevectors lie along the same axis, this corresponds to the case of three interacting 1D rolls.

$$\begin{aligned}
\nu f^3 &= \pi^5 \left(2.36 + 7.34 \frac{\mathcal{K}_2}{\Omega^2 \bar{C}^2}\right) f(0) \left(\left| f\left(\frac{\pi}{3}\right)\right|^2 + \left| f\left(\frac{2\pi}{3}\right)\right|^2 \right) \\
&\quad + \pi^5 \left(2.84 + 7.34 \frac{\mathcal{K}_2}{\Omega^2 \bar{C}^2}\right) f(0) \left| f(0) \right|^2 \quad \text{for a hexagonal array,} \\
&= \pi^5 \left(2.84 + 7.34 \frac{\mathcal{K}_2}{\Omega^2 \bar{C}^2}\right) f(0) \left| f(0) \right|^2 \quad \text{for rolls.} \qquad (49)
\end{aligned}$$

Note that (48) is positive definite, indicating that, in the absence of a quadratic term in the pattern equation, the bifurcation is supercritical.

Finally, we note that the coefficient in front of the time derivative in the pattern equation (44) is sign-altering:

$$\lambda = \Omega - 2 \frac{\bar{S}}{\Omega \bar{C}^2}. \qquad (50)$$

Thus, for a particular parameter regime λ may be negative or even vanish. As AW95 noted, this indicates the presence of a Hopf bifurcation. In this work, we do not consider this regime of parameter values and consider the direct mode only. A derivation of the full pattern equation in the presence of a Hopf bifurcation remains a topic for further research; in the meantime, our analysis is valid away from $\lambda = O(\delta)$ in parameter space.

6 Nascent chimney solutions to the pattern equation

For a stationary planform, the pattern equation (44) reduces to a non-linear inhomogenous ordinary differential boundary value problem and is easily handled by numerical mathematical tools such as MATLAB. Figure (5) depicts the solution in a periodic domain with representative values of $\rho = 3.9$, $\mu = 0.1$ and $\nu = 1.0$. See caption for details.

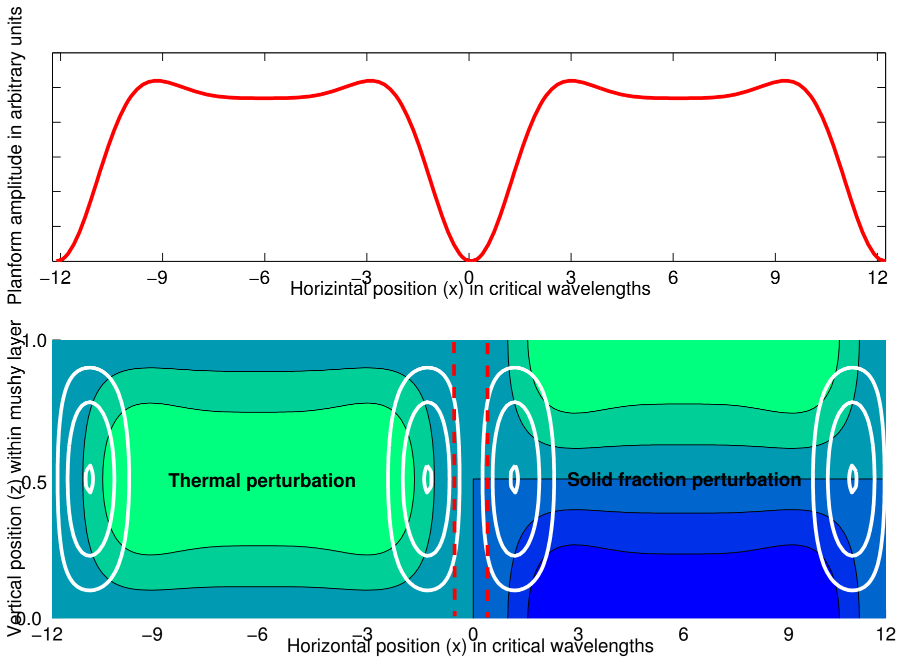

Figure 5: Stationary solutions for the planform (*top*) and perturbed fields (*bottom*). Horizontal position in each is measured in units of the critical wavelength. In the upper figure, the planform amplitude is plotted in arbitrary units. In the lower figure, the streamfunction is plotted in the x-z plane. Moving from left to right, the direction of rotation of the rolls is alternately clockwise and counter-clockwise. The region indicated by the vertical hatched lines represents a nascent chimney. In the background of the lower diagram, the temperature perturbation (*left*) and solid fraction pertubation (*right*) are indicated by contours. The units of these perturbations are arbitrary.

7 Discussion

As we have noted, the pattern equation derived in section (4) has the form of a Swift-Hohenberg equation with an additional quadratic term. The Swift-Hohenberg equation arises in a wide variety of physical, chemical and biological contexts and has a substantial literature associated with it (see Cross & Hohenberg [17] and references therein for a comprehensive review of this topic).

The quadratic term appearing in the pattern equation (44) breaks the symmetry between up and down. As we have noted, this quadratic term appears only for planforms made up of three rolls superposed at 120° to one another. If all three rolls have an equal amplitude, the unit cell is a hexagon. Thus, we recover the result of AH93 that the transition to three-dimensional hexagons is transcritical. The sign of the quadratic term determines whether there is up-flow or down-flow at the center of the hexagons.

We also note that the expression for the quadratic term (46) is proportional to $\bar{\mathcal{K}}_1$. Thus, symmetry-breaking between up-flow and down-flow at the center of hexagons is ultimately rooted in the non-Boussinesq effect of permeability variation with solid fraction. As $\bar{\mathcal{K}}_1$ is strictly positive on physical grounds, the overall sign of the quadratic term is determined by the planform $f(\alpha)$ itself, at least in this pared-down model.

Finally, it is amusing to note that while hexagons may determine which way is up by looking at the flow direction in their centre, rolls and all other planforms have no such method of distinguishing up from down. Translation of rolls and parallelograms by a half-cell merely exchanges the two directions. In this way, the hexagonal planform is fundamentally different from all other patterns: it is manifestly asymmetric.

Acknowledgements:

Thanks to the GFD Staff for an unforgettable experience, in particular: Neil B and John W for their constant encouragement; the Worster family for being so entertained and entertaining; Joe K and Louis H for permitting me to pick their esteemed brains; George V for introducing me to the national pastime, and his own; and Andrew Folwer (sic) for that beer I bought him. Thanks to Grae W for capturing my imagination in lectures, papers, and conversations. Special thanks to all of my fellow Fellows for their fellowship. Profound thanks to EAS for his guidance, supervision, and good company all summer. Finally, the author thanks SLK for permitting him to spend ten weeks away from her.

References

[1] Stephen H. Davis. *Theory of Solidification.* Cambridge University Press, 2001.

[2] M.G. Worster. Convection in mushy layers. *Ann. Rev. Fluid Mech.*, 29:91–122, 1997.

[3] Gustav Amberg and G.M. Homsy. Nonlinear analysis of bouyant convection in binary solidification with applications to channel formation. *J. Fluid Mech.*, 252:79–98, 1993.

[4] D.M. Anderson and M. Grae Worster. Weakly nonlinear analysis of convection in mushy layers during the solidification of binary alloys. *J. Fluid Mech.*, 302:307–331, 1995.

[5] D.M. Anderson and M. Grae Worster. A new oscillatory instability in a mushy layer during the solidification of binary alloys. *J. Fluid Mech.*, 307:245–267, 1996.

[6] F. Chen, J.W. Lu, and T.L. Yang. Convective instability in ammonium chloride solution directionally solidified from below. *J. Fluid Mech.*, 276:163–187, 1994.

[7] D.N. Riahi. On nonlinear convection in mushy layers part 1. oscillatory modes of convection. *J. Fluid Mech.*, 467:331–359, 2002.

[8] D.N. Riahi. On nonlinear convection in mushy layers. part 2. mixed oscillatory and stationary modes of convection. *J. Fluid Mech.*, 517:71–101, 2004.

[9] Peter Guba and M. Grae Worster. Nonlinear oscillatory convection in mushy layers. *J. Fluid Mech.*, 553:419–443, 2006.

[10] C.A. Chung and Falin Chen. Onset of plume convection in mushy layers. *J. Fluid Mech.*, 408:53–82, 2000.

[11] Peter Guba. On the finite-amplitude steady convection in rotating mushy layers. *J. Fluid Mech.*, 437:337–365, 2001.

[12] M.G. Worster. Instabilities of the liquid and mushy regions during solidification of alloys. *J. Fluid Mech.*, 237:649–669, 1992.

[13] A.C. Fowler. The formation of freckles in binary alloys. *IMA J. App. Maths*, 35(2):159–174, 1985.

[14] E.L. Ince. *Ordinary Differential Equations*. Dover Publications, Inc., 1926.

[15] W.V.R. Malkus and G. Veronis. Finite amplitude cellular convection. *J. Fluid Mech.*, 4:225–260, 1958.

[16] F.H. Busse. The stability of finite amplitude cellular convection and its relation to an extremum principle. *J. Fluid Mech.*, 30:625–649, 1967.

[17] M.C. Cross and P.C. Hohenberg. Pattern formation outside of equilibrium. *Rev. Mod. Phys.*, 65(3):851–1112, 1993.